Three-band Hubbard model: A Monte Carlo study

G. Dopf, A. Muramatsu,* and W. Hanke*
Physikalisches Institut, Universität Würzburg, Am Hubland, D-8700 Würzburg, Federal Republic of Germany
(Received 30 October 1989)

We have studied a two-dimensional multiband Hubbard model describing CuO_2 sheets in the high-T_c oxides. The simulations were performed for a grand-canonical ensemble on lattice sizes up to 16 unit cells of three atoms each and temperatures down to $k_B T \sim t/30$, where t is the Cu-O hybridization. For generally accepted values of the Hubbard coupling on the Cu sites $U_d \gtrsim 6t$, two different regimes can be distinguished in the magnetic properties of the model. In the half-filled band case we see for $\Delta > U_d/2$ ($\Delta = \varepsilon_p - \varepsilon_d$ being the charge-transfer energy) the formation of a correlation gap, as expected for a charge-transfer insulator. For $\Delta < U_d/2$, on the other hand, no gap is visible in the considered temperature region. In this (mixed-valence) situation only a very weak dependence of the magnetic structure form factor on doping is obtained, in contrast to the charge-transfer situation, where a strong decrease of the same quantity is observed for very low concentrations of dopant holes ($\delta \lesssim 0.05$). The existence of antiferromagnetic long-range order in the two different parameter regions is studied with finite-size scaling in the low-temperature regime. We also investigated the possibility of singlet formation between O holes and the Cu hole on one plaquette, as suggested by Zhang and Rice. The amplitude squared of such a singlet increases strongly as a function of doping, reaching saturation at $\delta \simeq 0.2$. Finally, we find evidence for an attractive pairing interaction only in the extended s-wave channel for $\delta = 0.2$ and $\beta \gtrsim 4/t$, although no phase transition to a superconducting state could be seen.

I. INTRODUCTION

The CuO_2 layers present in most of the ceramic superconductors[1] are the physical relevant elements for the remarkable magnetic properties and almost certainly for the high critical temperature as well. The long-range antiferromagnetic (AF) order observed in La_2CuO_4 and $YBa_2Cu_3O_6$ (the undoped phases)[2] is a clear indication of strong electronic correlation as first pointed out by Anderson[3] at the outset. Various mechanisms involving AF correlations, in an essential way, such as resonating valence bonds,[3,4] spin bags,[5] and spin fluctuations[6,7] have been proposed based on the one-band two-dimensional (2D) Hubbard model. However, spectroscopic data[8–10] show that the explicit inclusion of $2p$ orbitals on the O sites is necessary to properly describe the charge carriers introduced by doping, thus lending more support to multiband models as the one proposed by Emery.[11–13]

The strong interparticle correlations and fluctuations induced by Hubbard-type interactions make clear the need of rigorous or exact results beyond mean-field approximations. Due to the fact that exact analytic results are almost nonexistent for dimensions $D \geq 2$, an increasing amount of numerical work in the form of Monte Carlo simulations[14–23] and exact diagonalizations[24–26] was performed for both one- and multiband Hubbard models. Particularly interesting are the advances in Monte Carlo simulation techniques with stabilization algorithms[16,21,22,27,28] that allow now to study strongly correlated systems from the high-temperature limit down to essentially $T \to 0$. Nevertheless, a serious difficulty, due to the so-called minus-sign problem,[29] remains and does not allow for simulations in the low-temperature limit for arbitrary fillings in Hubbard models.[22]

We present in this article a Monte Carlo study of a multiband Hubbard model[11,12] for the CuO_2 layers. The motivation for this model and a detailed description are given in Sec. II. The algorithm used for our simulations is due to Blankenbecler, Scalapino, and Sugar[30] (BSS) and Hirsch,[14] improved with stabilization techniques[21,22,28] that allowed us to reach the low-temperature limit of the model. In order to make our paper self-contained we give a short survey of the simulation technique in Sec. III. The numerical results are described in Sec. IV. We first show (Sec. IV A) several results that demonstrate the ability and limitations of the algorithm in dealing with the three-band Hubbard model. The magnetic properties of the model are discussed in Sec. IV B. On the basis of these properties and the electronic compressibility we distinguish a charge-transfer from a mixed-valence type of behavior as a function of the parameter values. We further address the question, of whether AF long-range order is present in the system. In Sec. IV C we first study the formation of a local singlet between a hole on a Cu site and a hole on the four nearest-neighbor O sites. Zhang and Rice[31,32] suggested, that in the limit of strong repulsion on the Cu sites, the low-energy behavior of the multiband model can be described by such a singlet, allowing for a reduction to an effective one-band Hubbard model, or rather to a t-J model. In the second half of Sec. IV C we examine pairing correlation functions and susceptibilities. In the last Sec. V we summarize our numerical results.

II. THE MODEL

In order to model the CuO_2 layers, several features have to be taken into account. According to local-

density calculations[33] and spectroscopic data,[8,9] the relevant electronic elements should be given by $d_{x^2-y^2}$ orbitals on the Cu sites strongly hybridized with p_x or p_y orbitals on the oxygen atoms. Furthermore, a strong Coulomb repulsion on the Cu atoms must be present in order to account for the magnetic properties of the these materials. Moreover, the explicit inclusion of the O levels seems necessary since photoemission data[10] clearly show that the dopant holes have preferential O character. All the elements mentioned are contained in a multiband model that was originally proposed by Emery.[11]

The three-band model studied in this paper is given by the Hamiltonian,[11,12]

$$H=\sum_{\langle i,j\rangle\sigma} t_{ij}(d^{\dagger}_{i,\sigma}c_{j,\sigma}+\text{H.c.})+\sum_{\langle j,j'\rangle\sigma}\bar{t}_{jj'}(c^{\dagger}_{j,\sigma}c_{j',\sigma}+\text{H.c.}) +(\varepsilon_d-\mu)\sum_{i,\sigma} n^d_{i,\sigma}+(\varepsilon_p-\mu)\sum_{j,\sigma} n^p_{j,\sigma}+U_d\sum_i n^d_{i\uparrow}n^d_{i\downarrow} +U_p\sum_j n^p_{j\uparrow}n^p_{j\downarrow}\ . \tag{1}$$

The p-d hybridization between $d_{x^2-y^2}$ orbitals on the Cu sites and p_x or p_y orbitals on the O sites is given by[31]

$$t_{ij}=-t_{\text{Cu-O}}(-1)^{\alpha_{ij}}\ , \tag{2}$$

where $\alpha_{ij}=1$ if $j=i+\frac{1}{2}\hat{x}$ or $i-\frac{1}{2}\hat{y}$, and $\alpha_{ij}=2$ if $j=i-\frac{1}{2}\hat{x}$ or $i+\frac{1}{2}\hat{y}$. The phase factors in Eq. (2) are due to the d and p symmetry of the Cu and O orbitals, respectively (Fig. 1). The O-O hopping matrix element is defined in a similar way:

$$\bar{t}_{jj'}=t_{\text{O-O}}(-1)^{\beta_{jj'}}\ , \tag{3}$$

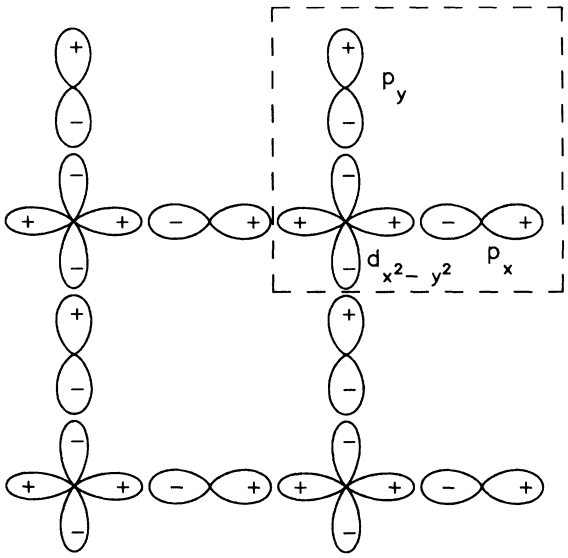

FIG. 1. Scheme of the underlying topology. On the copper sites we consider the $d_{x^2-y^2}$ orbitals and on the oxygen sites the p_x and p_y orbitals. The appropriate phase factors are also indicated.

where $\beta_{jj'}=1$ if $j'=j-\frac{1}{2}\hat{x}-\frac{1}{2}\hat{y}$ or $j'=j+\frac{1}{2}\hat{x}+\frac{1}{2}\hat{y}$, and $\beta_{jj'}=2$ if $j'=j-\frac{1}{2}\hat{x}+\frac{1}{2}\hat{y}$ or $j'=j+\frac{1}{2}\hat{x}-\frac{1}{2}\hat{y}$. The index i denotes the Cu sites and j the O sites. The local-orbital levels are given by ε_p and ε_d and the charge-transfer energy is $\Delta=\varepsilon_p-\varepsilon_d$. U_d and U_p are the Hubbard couplings on the Cu and O sites.

The three-band Hubbard model of Eq. (1) and variations of it were studied recently by several authors both analytically[11–13,31,32,34–36] and numerically.[18,23–25] In the following we briefly enumerate some essential points for a characterization of the Hamiltonian of Eq. (1), that emerged from the studies cited above.

The two key parameters of the system are the Coulomb repulsion U_d and the charge-transfer energy Δ. Based on the experience with transition metal oxides,[37] Zaanen and Oles[12] proposed several regimes in a U_d versus Δ diagram. For $U_d \gg \Delta$, a charge-transfer (CT) or a mixed-valence (MV) situation is present depending on whether Δ is much larger or of the order of the bandwidth W. In the opposite case ($U_d \ll \Delta$) a one-band Hubbard model is appropriate if $U_d \gg W$, whereas a metallic Brinkman-Rice[38] regime was suggested if $U_d \lesssim W$. Further mean-field calculations[39] based on the Hartree-Fock and Gutzwiller approximations were used to study the CT and MV regions that are thought to be relevant for the high-T_c materials.[12,39,40]

In the limit $U_d \gg \Delta \gg W$, the model can be reduced to a spin-Fermion system[12,13,41] with a fully developed localized spin on the Cu sites interacting with carriers on the O sites through a Kondo-like exchange:

$$J_{\text{Cu-O}}=t^2_{\text{Cu-O}}\left[\frac{1}{\Delta}+\frac{1}{U_d-\Delta}\right]\ . \tag{4}$$

Moreover, a Heisenberg exchange coupling between nearest-neighbor Cu spins is obtained in the next higher order,

$$J_{\text{Cu-Cu}}=\frac{4t^4_{\text{Cu-O}}}{\Delta^2}\left[\frac{1}{U_d}+\frac{1}{\Delta}\right]\ , \tag{5}$$

that would lead to a Neél state at half-filling (one hole per unit cell) and $T=0$. A further simplification was proposed by Zhang and Rice[31,32] who assumed that the doped carriers strongly bind to the Cu spins in a singlet state, thereby allowing for a mapping of the low-energy region of the model into a one-band Hubbard model or rather a t-J model. It was further proved by Zhang that this limit is exactly attained in the case where $\Delta\to\infty$, $U_d\to\infty$ but $U_d-\Delta$ is finite. Since, according to Eq. (5), this limit implies the cancellation of the antiferromagnetic exchange between Cu spins, the question arises of whether those singlets are still stable in the presence of low-lying magnetic excitations due to an exchange-coupling constant $J_{\text{Cu-Cu}}\sim 1000$ K.

In the MV itinerant situation, a few studies in the frame of a random-phase approximation (RPA) diagrammatic expansion were performed.[34,35] Antiferromagnetic long-range order is obtained at half-filling, but it survives up to fairly high-dopant concentrations if realistic values of U_d are used. Thus, the inclusion of higher-order

corrections (e.g., in the frame of a conserving approximation[42]) seems necessary. Nevertheless, a weak-coupling approach could still be qualitatively correct if the picture of a Fermi liquid, as suggested by some photoemission experiments,[43] is confirmed.

Unfortunately the parameters for the multiband models as obtained from *ab initio* calculations[40] are in an intermediate range. According to Ref. 40, the values of the parameters are the following: $t_{\text{Cu-O}} \approx 1.3-1.6$ eV, $U_d \approx 8.5-10.5$ eV, $\Delta \approx 3.6$ eV, $U_p \approx 4.0-7.5$ eV, $t_{\text{O-O}} \approx 0.65$ eV, and $U_{pd} \approx 0.6-1.2$ eV. The last parameter corresponds to a Coulomb repulsion between nearest-neighbor Cu and O sites. We did not include such an interaction in our model, since the corresponding coupling is apparently small. Furthermore, both weak- and strong-Coulomb calculations[35,36] did not show any dramatic influence due to U_{pd}. Nevertheless, such an operator could be relevant in the presence of U_p as suggested by exact diagonalization results.[24] From the values above, it is rather difficult to decide *a priori* whether the (strong-coupling) CT or the (weak-coupling) MV picture is more appropriate for the high-T_c materials. We will address this question in Sec. IV B by considering the magnetic properties of the system and the opening of a gap for different parameter sets.

III. THE SIMULATION

In this section we give a short description of the algorithm used to perform finite-temperature studies of a grand canonical ensemble. The basic developments are due to Blankenbecler, Scalapino, and Sugar[30] (BSS) and Hirsch,[14] who applied the algorithm for the first time to the Hubbard model. Further improvements, that allow for low-temperature simulations, were achieved very recently.[22]

Our aim is to calculate the expectation value of a physical observable $\mathcal{O}$, defined by

$$\langle \mathcal{O} \rangle = \frac{\mathrm{Tr}(\mathcal{O} e^{-\beta H})}{\mathrm{Tr}(e^{-\beta H})} . \tag{6}$$

To this end a small imaginary time step $\Delta\tau$ ($\beta = L\Delta\tau$) is introduced and, by means of the Trotter formula,[44] the partition function can be written in the form

$$\begin{aligned} Z &= \mathrm{Tr}(e^{-\beta H}) \\ &= \mathrm{Tr}(e^{-\Delta\tau K_1} e^{-\Delta\tau K_2} e^{-\Delta\tau V_d} e^{-\Delta\tau V_p})^L + O((\Delta\tau)^2) . \end{aligned} \tag{7}$$

The first exponent corresponds to the *p-d* hybridization,

$$K_1 = \sum_{\langle i,j \rangle \sigma} t_{ij} (d^\dagger_{i,\sigma} c_{j,\sigma} + \text{H.c.}) = \sum_{\langle i,j \rangle \sigma} d^\dagger_{i,\sigma} k^{(1)}_{i,j} c_{j\sigma} , \tag{8}$$

and the second exponent is due to the direct O-O hopping,

$$\begin{aligned} K_2 &= \sum_{\langle j,j' \rangle \sigma} \bar{t}_{jj'} (c^\dagger_{j,\sigma} c_{j',\sigma} + \text{H.c.}) \\ &= \sum_{\langle j,j' \rangle \sigma} c^\dagger_{j,\sigma} k^{(2)}_{j,j'} c_{j'\sigma} . \end{aligned} \tag{9}$$

The other terms refer to the potential and interaction parts on both Cu and O sites:

$$V_\alpha = U_\alpha \sum_m n^\alpha_{m,\uparrow} n^\alpha_{m,\downarrow} + (\varepsilon_\alpha - \mu) \sum_{m,\sigma} n^\alpha_{m,\sigma} , \tag{10}$$

where α corresponds to d or p depending on whether m is a Cu or O site.

Now a discrete Hubbard-Stratonovich transformation[45] is applied to the interaction terms in order to bring them into a bilinear form:

$$\begin{aligned} &\exp(-\Delta\tau U_\alpha n^\alpha_{m,\uparrow} n^\alpha_{m,\downarrow}) \\ &\quad = \tfrac{1}{2} \mathrm{Tr} \sigma_{m,l} \exp[\lambda_\alpha \sigma_{m,l} (n^\alpha_{m,\uparrow} - n^\alpha_{m,\downarrow}) \\ &\qquad - \tfrac{1}{2} U_\alpha \Delta\tau (n^\alpha_{m,\uparrow} + n^\alpha_{m,\downarrow})] , \end{aligned} \tag{11}$$

with

$$\tanh^2\left[\frac{\lambda_\alpha}{2}\right] = \tanh\left[\frac{\Delta\tau U_\alpha}{4}\right] . \tag{12}$$

The Hubbard-Stratonovich transformation must be performed on each lattice site m and at each time slice l, therefore the auxiliary Ising variable $\sigma_{m,l}$ has the corresponding two space-time indices. Since the original Hamiltonian was mapped into a free fermion system interacting with a fluctuating classical field, the quantum-mechanical trace can be now performed. The result is[30,14]

$$Z = \sum_{\{\sigma_{m,l}\}} (\det \mathcal{O}^+ \det \mathcal{O}^-) , \tag{13}$$

with

$$\mathcal{O}^\pm = I + B^\pm_L B^\pm_{L-1} \cdots B^\pm_1 \tag{14}$$

and

$$B^\pm_l = e^{-\Delta\tau k^{(1)}} e^{-\Delta\tau k^{(2)}} e^{v^\pm_1(l)} e^{v^\pm_2(l)} . \tag{15}$$

In Eq. (15) we denoted

$$v^\pm_\alpha(l) = \delta_{m,m'} \left[\pm \lambda_\alpha \sigma_m(l) + \Delta\tau \left[\mu - \varepsilon_\alpha - \frac{U_\alpha}{2} \right] \right] . \tag{16}$$

The Fermion determinants $\det\mathcal{O}^\pm$ are functionals of the Ising field $\sigma_{m,l}$. Notice that according to BSS only matrices with space indices are necessary, since the temporal part is taken into account through a time-evolution operator.[30,14]

A sequence of Hubbard-Stratonovich fields $\{\sigma_{m,l}\}$ is generated, which is distributed according to $|\det\mathcal{O}^+ \det\mathcal{O}^-|/Z$ using a standard Monte Carlo method. We reject or accept a spin flip in the 3D Ising lattice according to a heat-bath algorithm.[46] The probability for acceptance is

$$P = \frac{R^+ R^-}{1 + R^+ R^-} , \tag{17}$$

with

$$R^\pm = \frac{|(\det\mathcal{O}^\pm)_{\text{new}}|}{|(\det\mathcal{O}^\pm)_{\text{old}}|} . \tag{18}$$

The determinant $(\det\mathcal{O}^+)_{\text{new}}$ differs from $(\det\mathcal{O}^+)_{\text{old}}$ through the flipped Ising spin.

In these expressions the absolute value is taken since the fermionic determinants have no definite sign. Accordingly, the average for a certain quantity A is given by

$$\langle A\rangle=\frac{\sum_{\{\sigma_{m,l}\}} A\,\mathrm{sgn}(\det\mathcal{O}^+\det\mathcal{O}^-)|\det\mathcal{O}^+\det\mathcal{O}^-|}{\sum_{\{\sigma_{m,l}\}}\mathrm{sgn}(\det\mathcal{O}^+\det\mathcal{O}^-)|\det\mathcal{O}^+\det\mathcal{O}^-|}\ . \quad (19)$$

In the case where the average sign in the denominator of Eq. (19) is small ($\sim 10^{-2}$), large fluctuations will completely deteriorate the measurements. This so-called "minus-sign problem" appears as the temperature is lowered.[29]

The algorithm described delivers only reliable results for $\beta\leq 4/t$. For lower temperature (larger β or L) rounding off errors seriously affect the accuracy with which the product $B_L^{\pm}B_{L-1}^{\pm}\cdots B_1^{\pm}$ can be calculated, since very large and very small numbers are spread over the whole matrix. This problem can be overcome by using matrix factorization methods, for instance, the Gram-Schmidt orthogonalization procedure.[22] The product $B_L^{\pm}B_{L-1}^{\pm}\cdots B_1^{\pm}$ is split in a product of L/k terms, which themselves are numerically accurate, because we choose a small enough k. Each term can be factorized as

$$B_{n+k-1}^{\pm}\cdots B_n^{\pm}=U^{\pm}D^{\pm}R^{\pm}\ . \quad (20)$$

$U^{\pm}$ is an orthogonal matrix, $D^{\pm}$ a diagonal, and $R^{\pm}$ an upper triangular matrix. The diagonal matrix, which incorporates new elements with large variations in their magnitude, is easy to handle under numerical operations (especially under inversion). The practice shows that the matrix $R^{\pm}$ is well conditioned, whereas $U^{\pm}$ is well conditioned since it is orthogonal.

With this modified algorithm we can reach inverse temperatures as low as $\beta=30/t$ or even lower ones. This improvement allows for simulations of electronic systems down to essentially $T=0$, except in cases where the minus-sign problem appears. In the simulation of a three-band Hubbard model, it is our experience that minus signs play an important role for inverse temperatures $\beta\gtrsim 10/t$ and for hole doping $\delta\neq 0$. Notice that in this case no particle-hole symmetry is present for $\delta=0$, as is the case for the one-band Hubbard model.

IV. NUMERICAL RESULTS

A. Tests

In order to demonstrate the ability of the implemented algorithm, we present here some test results. We consider first the spin-spin correlation function

$$S(l_x,l_y)=\frac{1}{N}\sum_i\langle(n_{i\uparrow}-n_{i\downarrow})(n_{i+l\uparrow}-n_{i+l\downarrow})\rangle\ , \quad (21)$$

where the index i corresponds to the copper sites and N is the number of elementary cells. As can be seen in Fig. 2,

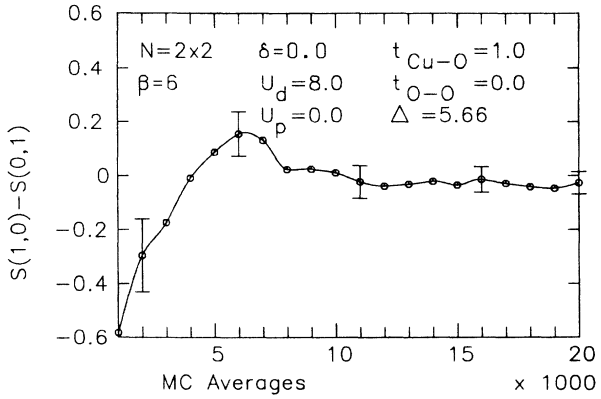

FIG. 2. Asymmetry in the spin-spin correlation function versus Monte Carlo averages. The difference for the nearest-neighbor spin-spin correlation in the $\hat{\mathbf{x}}$ and $\hat{\mathbf{y}}$ direction is negligible for more than $\sim$8000 MC averages. Here and in the following data the solid lines serve only as a guide for the eye.

for a few thousand Monte Carlo (MC) averages there is still a considerable difference in the nearest-neighbor spin-spin correlation function when comparing the $\hat{\mathbf{x}}$ ($S(l_x=1,l_y=0)$) and the $\hat{\mathbf{y}}$ direction ($S(l_x=0,l_y=1)$). The quadratic symmetry of the lattice is numerically restored only after $\sim$8000 averages for relative large values of U_d. The parameters chosen in Fig. 2 are such (system size $N=2\times 2$ unit cells; $U_d=8.0$; $t_{\text{Cu-O}}=1.0$; $\Delta=5.66$; doping $\delta=0.0$; all other parameters are zero) that almost one hole is located on the copper site.

Figure 3 shows the staggered magnetization

$$m=\frac{1}{N}\sum_i(-1)^i\langle n_{i\uparrow}^d-n_{i\downarrow}^d\rangle \quad (22)$$

as a function of MC averages. The sum is carried out only at the Cu sites. Reliable results can be obtained for

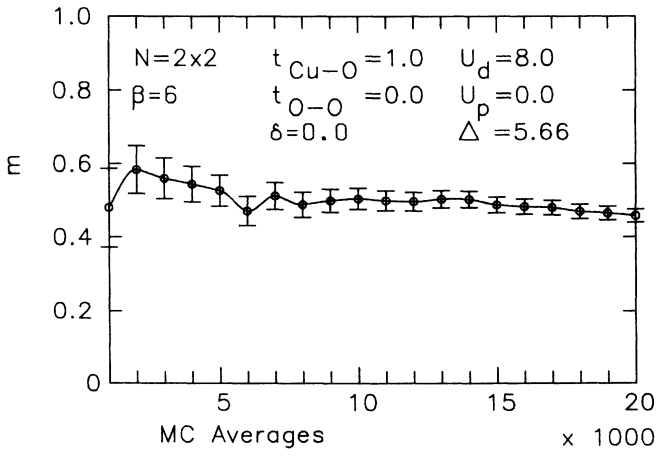

FIG. 3. Staggered magnetization as a function of Monte Carlo averages. Statistics of a few thousand averages is sufficient to obtain convergence.

less MC steps, than in the case of Fig. 2, since for such local quantities the statistics is better.

Next we present some results concerning the magnetic structure form factor

$$S(\mathbf{q})=\sum_{l} e^{i\mathbf{q}\cdot\mathbf{l}}S(l_x,l_y)\ . \tag{23}$$

The data plotted in Fig. 4 show that, by means of the low-temperature algorithm described above, it is possible to reach the $T=0$ limit of the model Hamiltonian, Eq. (1), since for different values of U_d and Δ, the MC data converge to the triangles at $\beta=34/t$, which were calculated with an exact diagonalization Lanczos method.

The results we present in the following were obtained with $\sim$2000 averages and checked eventually with some $\sim$1000 averages more. It is our experience that qualitative differences can already be seen (for the considered parameter regions) with this statistics. Furthermore, a value of $\Delta\tau=0.125$ was used for the simulations with $U_d=6$. The units of energy are given by $t_{\text{Cu-O}}=1.0$.

B. Magnetic properties

First we discuss the magnetic properties of the system described by Eq. (1), since antiferromagnetism is a clear experimental feature for the Cu-based superconductors in the undoped case. We will concentrate mainly in two different parameter sets such that at half-filling one corresponds to a hole almost localized on the Cu site, whereas for the other one the hole is evenly spread in the unit cell. These two regimes will be then identified as the CT and MV regions discussed in Sec. II.

We consider first the squared local magnetic moment

$$\langle S_z^2\rangle=S(0,0)=\frac{1}{N}\sum_i\langle(n_{i\uparrow}^d-n_{i\downarrow}^d)^2\rangle\ , \tag{24}$$

where the sum is carried out only on the Cu sites.

Figure 5 shows the squared moment $\langle S_z^2\rangle$ as a function of U_d for one hole per unit cell (doping $\delta=0$). The charge-transfer energy was chosen as $\Delta=2U_d/3$, in order to have, for larger U_d, a well-localized spin on the Cu sites (in the case of $U_d=6$ the hole occupation number on Cu is $\langle n_{\text{Cu}}\rangle\approx0.85$). For $U_d\geq6$ the curve tends to saturate (for $\Delta=2/3U_d$ and $U_d\to\infty$ it follows that $\langle S_z^2\rangle\to1$). Next we consider $\langle S_z^2\rangle$ as function of Δ for a value of $U_d=6$ (Fig. 6). It can be seen that for very small Δ, a moment is obtained that is very close to the value of a noninteracting system ($U_d=0$ in Fig. 5). On the other hand, a well-developed magnetic moment is present for $\Delta>U_d/2$. The inverse temperature for the calculation in Fig. 6 is $\beta=3/t$. This is enough for a qualitative discussion, since the local magnetic moment is very insensitive with respect to temperature. We have checked our measurements of the local magnetic moment in a 2×2 system with data of an exact diagonalization program and found very good agreement. For a system size $N=4\times4$ and inverse temperature $\beta=3/t$, we have $\langle S_z^2\rangle=0.830\pm0.002$, whereas for $\beta=28/t$, $\langle S_z^2\rangle=0.834\pm0.001$. The value

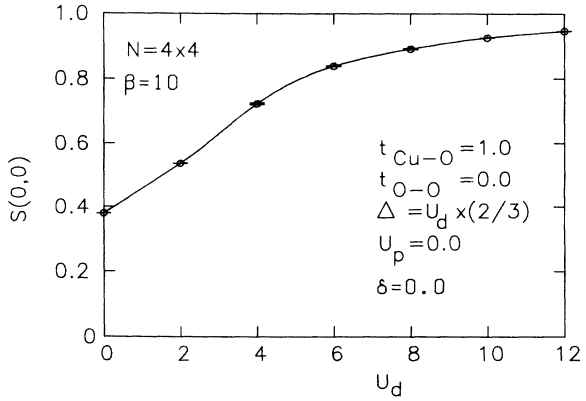

FIG. 5. Local magnetic moment squared $S(0,0)=\langle S_z^2\rangle$ on the Cu sites as a function of U_d. The curve saturates for values of the coupling $U_d\geq6$.

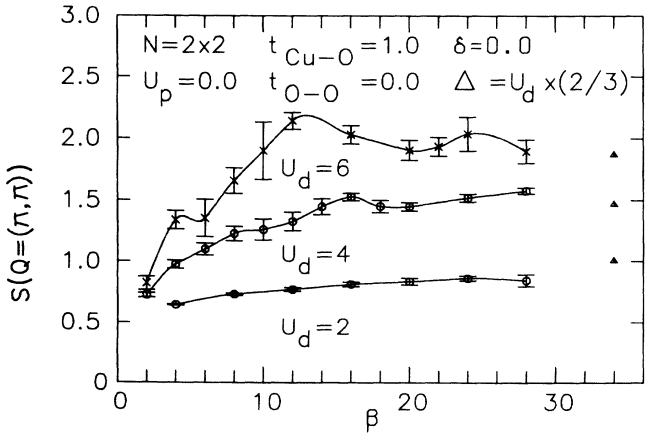

FIG. 4. Structure form factor $S(\mathbf{q})$ at the wave vector $\mathbf{q}=(\pi,\pi)$. The triangles at $\beta=34/t$ are exact diagonalization results ($T=0$). For low temperatures (high values of β) the MC results converge to the exact data.

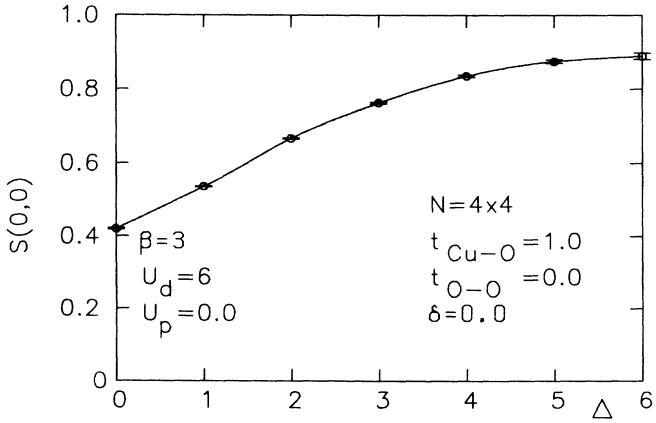

FIG. 6. $\langle S_z^2\rangle$ as function of Δ. Saturation is reached for $\Delta\gtrsim4$.

from the exact diagonalization is 0.804.

In the following the Coulomb repulsion on Cu will be fixed at $U_d=6$ since, from the data of Figs. 5 and 6, it is seen that with this value it is already possible to distinguish the two different situations. Moreover, such a value is in agreement with *ab initio* calculations made to determine the parameters of multiband models.[40] For the localized regime a value of $\Delta=4$ ($2U_d/3$) will be taken and for the itinerant region, $\Delta=1$ ($U_d/6$). The occupation number on the Cu site for the latter parameter set ($U_d=6$, $\Delta=1$) is $\langle n_{\mathrm{Cu}}\rangle\approx 0.56$. Furthermore, the local moment squared in this case is nearly the same as for $U_d=2$, $\Delta=1.33$. In both cases we obtain $\langle S_z^2\rangle\approx 0.54$, corresponding to a weak-coupling itinerant picture. Finally we would like to mention that for $\Delta=U_d/6$ no saturation can be found in $\langle S_z^2\rangle$ even for $U_d\sim 12$.

Figure 7 shows $\langle S_z^2\rangle$ as a function of doping for both cases. Similar to the experimental results,[47,48] they show almost no dependence on doping. Unfortunately, only results about the integrated intensity have been published so far (to our knowledge), making it difficult to compare the values of the local moment obtained for the simulation with experimental ones.

A dramatic difference between the two cases $\Delta=4$ and $\Delta=1$ appears in the magnetic structure form factor [Eq. (23)] when studied as a function of doping (Fig. 8). For $\Delta=4$, $S(\mathbf{q})$ drops rapidly at very small doping ($\delta\lesssim 0.05$), whereas for $\Delta=1$ almost no dependence is observed. These data were taken at an inverse temperature $\beta=10/t$; the lowest temperature we could reach without having massive minus-sign problems at finite doping, especially for $\delta\sim 0.1$. It is interesting to observe that the range of doping where $S(\mathbf{q})$ strongly decreases [curve (a) in Fig. 8], is in qualitative agreement with experiments where antiferromagnetic order ceases to be observed at $\delta\sim 0.05$.

In order to address the question whether long-range antiferromagnetic order is present in the different parameter regions, we performed finite-size studies. Due to the computational time required, only systems up to 16 unit cells ($N=4\times 4$) could be considered. Figure 9 shows $S(\pi,\pi)$ for systems with 4, 10 , and 16 unit cells. The

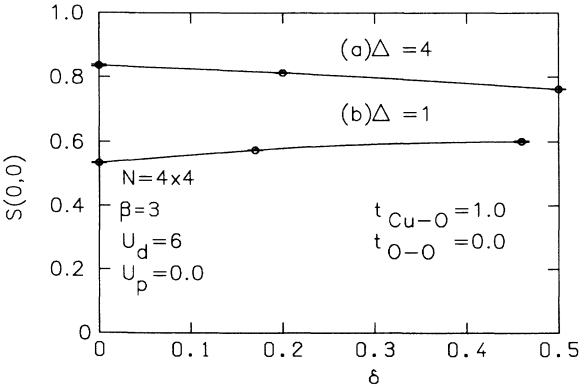

FIG. 7. $\langle S_z^2\rangle$ versus doping. Almost no dependence on doping can be seen in both cases.

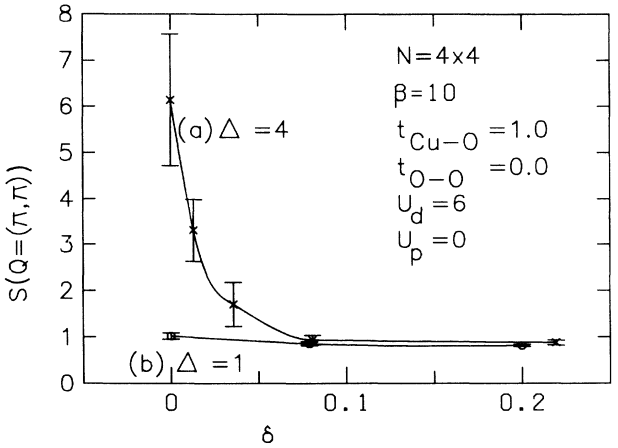

FIG. 8. Magnetic structure form factor versus doping. The CT case shows a strong decrease for very small doping $\delta\lesssim 0.05$, whereas the MV curve shows almost no dependence.

system with 10 unit cells has the geometry proposed originally by Oitmaa and Betts.[49] In order to ensure that the ground-state properties are reflected in our simulations, an inverse temperature of $\beta=28/t$ was used. Both in this case and in Fig. 10 we performed the finite-size studies at the temperature where $S(\pi,\pi)$ saturates (for the largest system size considered) as β is increased. Although in the one-band Hubbard model the data scale as $1/\sqrt{N}$ (Refs. 24 and 22), the best fit in our case was obtained for a $1/N$ law. This discrepancy is possibly due to the small sizes used in the simulations. Nevertheless, one could speculate that the system studied is not well described by the spin-$\frac{1}{2}$ Heisenberg model currently obtained in the strong-coupling expansions of the Hubbard model, and that other operators may also be relevant. Simulations with better statistics and larger system sizes are presently carried out in order to shed light in this point. A finite

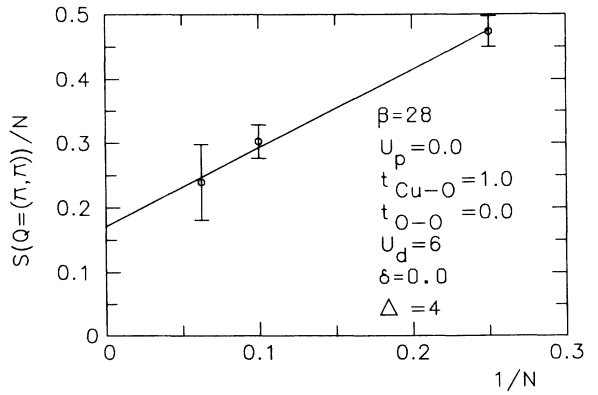

FIG. 9. Finite-size extrapolation of the structure form factor $S(\mathbf{q}=(\pi,\pi))$ in the "strong-coupling" case for zero doping. The extrapolation to $N\rightarrow\infty$ indicates the existence of long-range antiferromagnetic order. The inverse temperature is $\beta=28/t$ in order to ensure that the system is in the limit of $T=0$.

point. A finite value of $m_z^2=0.17\pm0.06$ is obtained from the extrapolation to $N\rightarrow\infty$, indicating that long-range order is present.

We consider next our mixed-valence set of parameters ($U_d=6$ $\Delta=1$). We can see in Fig. 10 that for this case AF long-range order is also present. The extrapolated value is $m_z^2=0.06\pm0.01$. It is about 3 times smaller than the one obtained from Fig. 9. These results would imply that a spin-density wave is also present in the "weak-coupling" limit in agreement with perturbative results.[34,35]

Finally, Fig. 11 shows results with the same parameters as in Fig. 10, but now the doping is $\delta=0.2$. We see that the extrapolated value of m_z^2 is practically zero ($m_z^2=0.007\pm0.004$), indicating the vanishing of the AF long-range order under doping. However, currently it is not possible to go beyond a qualitative description, keeping in mind the size of the simulated systems used for the extrapolation.

We conclude this section with a study of the metallic and insulating phases of the system that complements the description of the magnetic properties discussed earlier. First we consider the case $U_d=6$, $\Delta=4$. In Fig. 12(a) we have plotted the total hole occupation number per elementary cell as a function of the chemical potential μ. With decreasing temperature a large region develops where $\langle n\rangle$ remains constant as the chemical potential is moved. Therefore, for this parameter set the system is in the CT regime with an appreciable gap opening at low enough temperatures ($\beta=10/t$).

A quantitative measure of a gap is given by the electronic compressibility

$$\kappa=\frac{1}{\langle n\rangle^2}\frac{\partial\langle n\rangle}{\partial\mu}\ . \tag{25}$$

We have taken numerically the derivative of the curve in Fig 12(a) and calculated κ. Figure 12(b) shows very clearly that a gap opens at sufficiently low temperatures. In that case κ is 0 over a very broad range of values of μ. The estimated gap is $\Delta_{CT}\approx1.2$. This is a lower bound since the data were taken at a finite temperature. Unfortunately we were not able to go to much lower tempera-

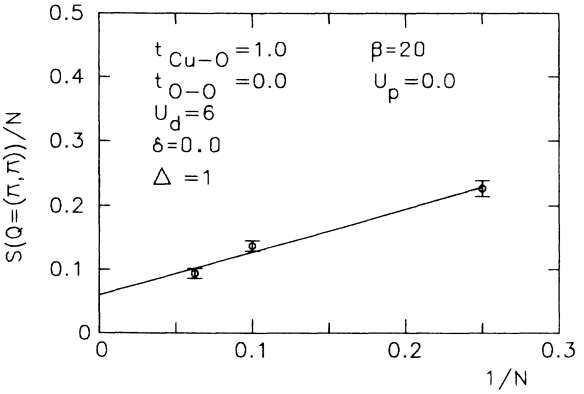

FIG. 10. Finite-size study for the case $U_d=6$, $\Delta=1$, and $\delta=0$. A finite staggered magnetization results from the extrapolation.

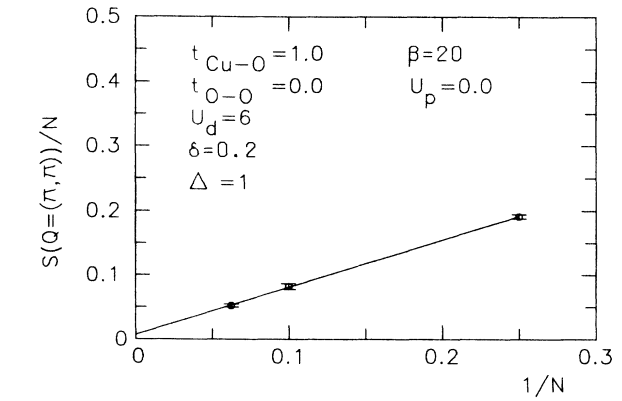

FIG. 11. Finite-size study for the case $U_d=6$, $\Delta=1$, and $\delta=0.2$. For finite doping a vanishing magnetization results from the extrapolation.

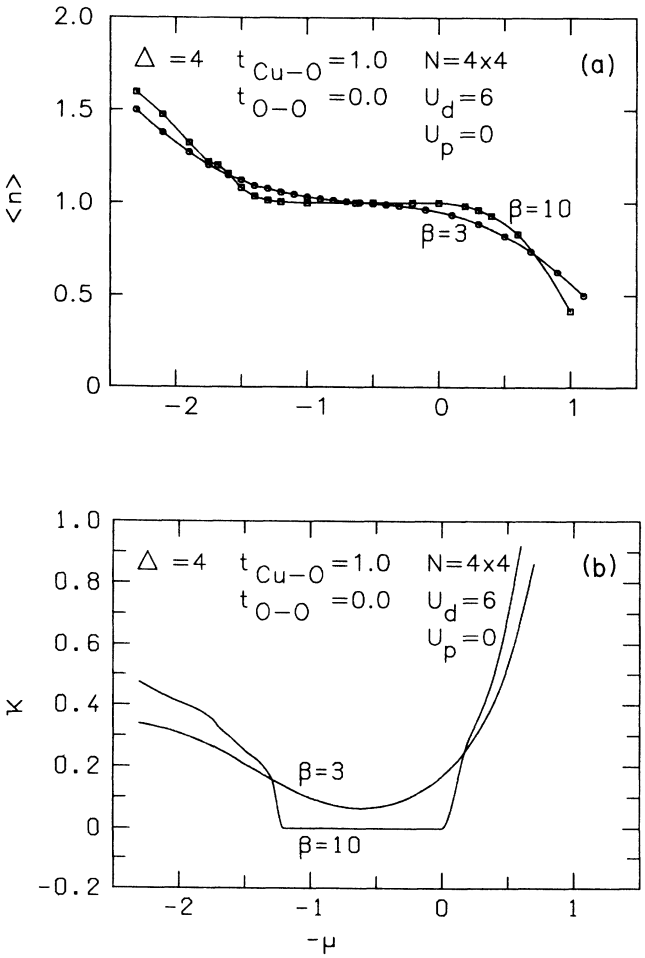

FIG. 12. (a) Hole occupation number per elementary cell as a function of chemical potential. A large charge-transfer gap develops for low enough temperatures ($\beta=10/t$). (b) Electronic compressibility κ as function of chemical potential. The formation of a gap with decreasing temperature is clearly visible.

tures ($\beta=20/t$) due to the minus-sign problem. Nevertheless it is interesting to notice that the value obtained from the simulation agrees very well with the corresponding experimental value ($\Delta_{\text{CT-expt}}\approx 1.7$ eV).[50]

Figure 13 shows the same quantities as the previous case but now for $U_d=6$ and $\Delta=1$. It can be seen that no feature indicative of a gap is present even at the lowest temperature. In particular, the compressibility κ is clearly nonzero. This fact shows that we are in the MV region, where the gap—if it exists—should be much smaller than $k_B T=0.1$. Furthermore, it explains the difference between curves (a) and (b) in Fig. 8. Whereas in the CT case ($U_d=6$, $\Delta=4$) an appreciable gap is present, also in agreement with the large value of m^2 obtained from the finite-size study in Fig. 9, the MV situation is almost not perturbed by doping since no gap is observable at the temperatures reached. However, a hint for the presence of a gap also in the MV regime is given by the finite value obtained for m^2 from Fig. 10. This may indicate that at $\beta=20/t$ a gap structure can already be observed. Further studies for lower temperatures in this regime are presently being carried out. Nevertheless, it is interesting to notice that although the values of the parameters seem to lie in an intermediate coupling region, a clear difference between a CT and a MV regime can be seen.

C. Correlation functions and susceptibilities

In this section we first discuss the formation of a singlet between a hole on a Cu site and a hole in a symmetric combination of the four nearest-neighbor O sites, as introduced by Zhang and Rice (ZR).[31,32] This picture was originally suggested in the parameter region where a spin is localized on the Cu site and the dopant hole resides mainly on the O sites. It was proved to be exact in the limit $U_d\to\infty$, $\Delta\to\infty$ but $U_d-\Delta$ finite,[32] a limit where the antiferromagnetic interaction between Cu sites is canceled. In the following we study such a singlet in the CT region but for more realistic parameters.

We consider the propagator for those singlets defined by

$$G_s(x,\tau)=\frac{1}{N}\sum_i \langle \psi^\dagger(x_i+x,\tau)\psi(x_i)\rangle \ , \tag{26}$$

where $\psi(x)$ corresponds to a singlet buildup by a Cu hole and a symmetric combination of a hole on the four nearest neighbors to the Cu site:

$$\psi(x_i)=\frac{1}{\sqrt{2}}(d_{i\uparrow}P_{i\downarrow}-d_{i\downarrow}P_{i\uparrow}) \tag{27}$$

with

$$P_{i\sigma}=\tfrac{1}{2}\sum_{j\text{NN}i}(-1)^{\alpha_{ij}}c_{j\sigma} \ , \tag{28}$$

where α_{ij} was defined in Eq. (2). Figure 14 shows the amplitude for a local singlet $G_s(0,0)$ in the localized region as a function of doping for both the interacting ($U_d=6$, circles) and noninteracting case. It can be seen that only for $\delta\geq 0.2$ an appreciable enhancement is obtained. The noninteracting case corresponds to $U_d=0$ in Eq. (1), but with Δ corrected in such a way that the occupation numbers for both Cu and for O are equal to the ones when $U_d\neq 0$. In this way we take into account the Hartree-type contributions. The remaining difference between the two curves should give a measure of the tendency for the formation of a local singlet due to the interaction. The almost linear increase with doping seems to indicate that the more holes are added, the more singlets are built up. This conclusion is somewhat dangerous since, for the parameters considered here, part of the holes introduced by doping go into the Cu sites.

Figure 15 shows the same data as in Fig. 14 but now normalized to the number of holes present in oxygen. For small doping concentrations, an increase is observed up to $\delta\approx 0.2$ where saturation sets in. This indicates that the amplitude of the singlets itself also increases with doping until a maximum is reached. Thus, from the data obtained to this point, we infer that in the parameter re-

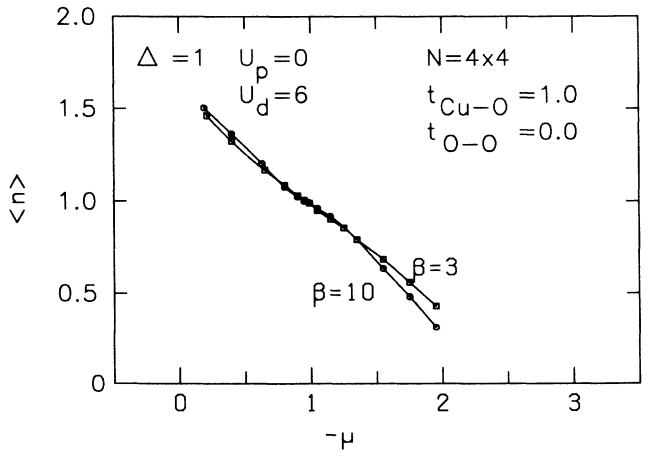

FIG. 13. Hole occupation number per elementary cell as a function of chemical potential. In this case no feature indicative of a gap is observed at half-filling (1 hole per cell).

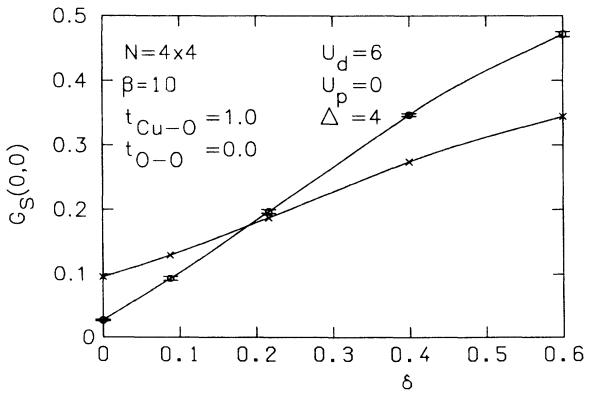

FIG. 14. Squared amplitude for a local Cu-O singlet versus doping. Circles denote the interacting case; crosses the noninteracting one. An enhancement of the interacting curve is obtained for $\delta\geq 0.2$ only.

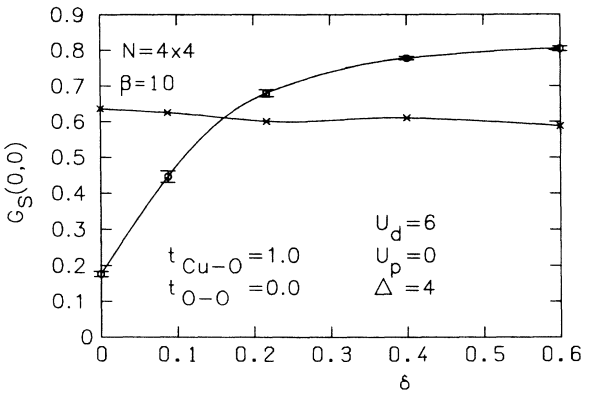

FIG. 15. Squared amplitude for a local Cu-O singlet, normalized by $2\langle n_p \rangle$, versus doping. The amplitude increases with doping until at $\delta \approx 0.2$ saturation sets in.

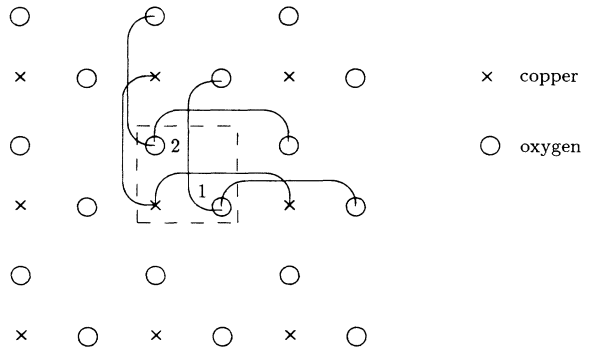

FIG. 17. Contributions to the calculated extended s-wave singlet.

gion under study, the ZR singlets begin to dominate after a certain dopant concentration is reached. This concentration is well beyond the values where antiferromagnetic correlations are important. In order to further clarify this situation, calculations with larger U_d (where the Cu local moment reaches the maximum value $\langle S_z^2 \rangle = 1$) are currently being carried out. The temperature behavior of the Cu-O singlet is shown in Fig. 16. Since the essential coupling for building the singlet is the relatively large $J_{\text{Cu-O}}$, the curves are nearly constant.

Next we present some results related to the possibility of superconductivity in the present system. We first consider the pair correlation function for the order parameter in the extended s-wave channel (SPX)

$$P(\tau,\mathbf{q}) = \frac{1}{N} \sum_{i,j} e^{i\mathbf{q}(\mathbf{R}_i - \mathbf{R}_j)} \langle \hat{\mathcal{O}}_i(\tau) \hat{\mathcal{O}}_j^{\dagger}(0) \rangle \ , \tag{29}$$

where

$$\hat{\mathcal{O}}_i = \frac{1}{\sqrt{2}} \frac{1}{\sqrt{6}} \sum_{\substack{m=1,2,3 \\ l=x,y}} (a_{i\uparrow}^m a_{i+\hat{l}\downarrow}^m - a_{i\downarrow}^m a_{i+\hat{l}\uparrow}^m) \ , \tag{30}$$

with $a_i^1 = d_i$, $a_i^2 = p_i^1$, and $a_i^3 = p_i^2$. Figure 17 shows the combinations taken into account by the operator $\hat{\mathcal{O}}_i$. The total singlet, as written in Eq. (30), is constructed as a superposition of 6 contributions, which are denoted as lines in Fig. 17. Each contribution is given by sites belonging to different unit cells. These cells are separated by one lattice vector in the $\hat{x}$ or $\hat{y}$ direction. This ensures the correct form factor $f_{s^*} = \cos(k_x) + \cos(k_y)$ for the total singlet. The oxygen atoms in the elementary cell are marked with the numbers 1 and 2 for distinction.

For the mixed-valence case Fig. 18 shows the equal-time pair-correlation function ($\tau = 0$, $\mathbf{q} = 0$) as defined in Eq. (29). The noninteracting case was again calculated with a Hartree correction (as in the case of the Cu-O singlets), i.e., with Δ modified in such a way that the same occupation numbers are obtained as in the interacting case. An enhancement is seen for $T \lesssim 0.25$. We have also studied d-wave pair-correlation functions and

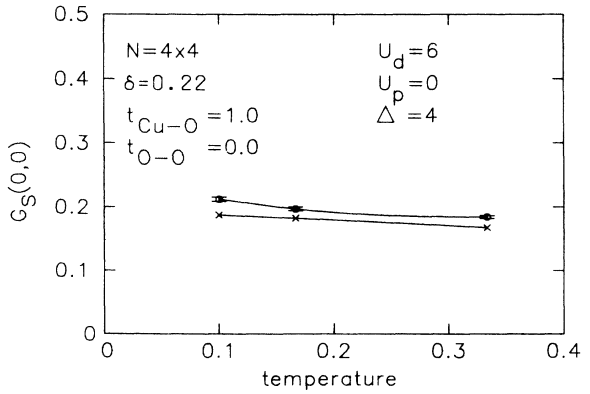

FIG. 16. Temperature behavior of the Zhang-Rice singlet. The calculated curve remains nearly constant in the considered temperature region since the relevant coupling $J_{\text{Cu-O}}$ is large compared to the temperature.

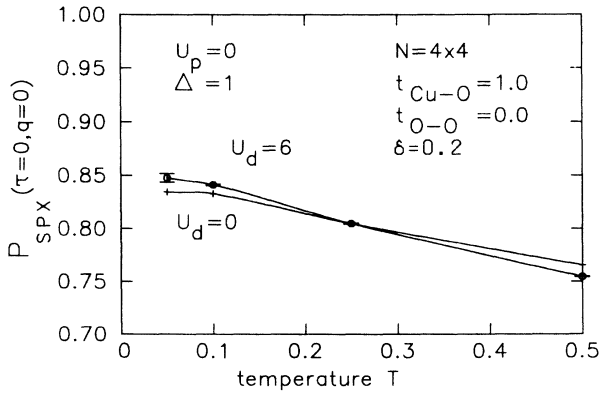

FIG. 18. Equal-time correlation function for extended s-wave pairing in the mixed-valence case. Enhancement is obtained for $T \lesssim 0.25$.

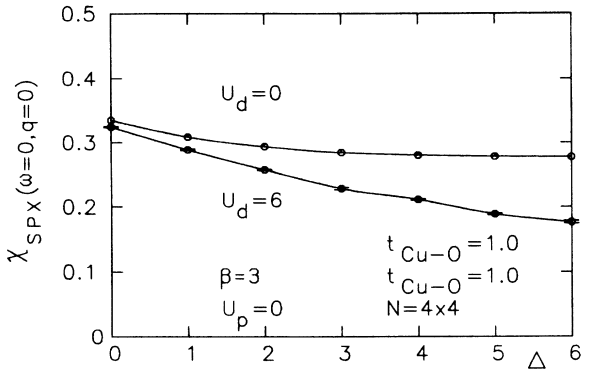

FIG. 19. Extended s-wave susceptibility versus Δ. The difference between the curves calculated with and without Hubbard repulsion is smallest for $\Delta=0$. Therefore the region with small Δ seems to be the best to search for superconductivity within the model.

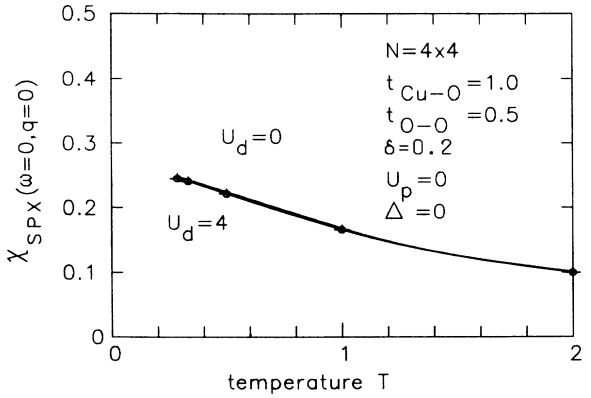

FIG. 21. Pairing susceptibility for the extended s-wave channel. The parameters are the same as in Fig. 20 except that now $t_{O\text{-}O}=0.5$.

different p-wave and s-wave cases, but the extended s wave is the only channel where a fluctuation enhancement in the $\tau=0$ correlation function can be observed. In the localized case we could not find such an enhancement up to $\beta=10/t$. Due to minus-sign problems we were not able to simulate lower temperatures.

Since the equal-time correlation functions give only a measure of the overlap of pair wave functions, the above results can only be considered as a hint for superconductivity. The phase transition to a superconducting state will be shown by a divergence of the susceptibility

$$\chi(\omega=0,\mathbf{q})=\int_0^\beta d\tau\, P(\tau,\mathbf{q})\ . \tag{31}$$

We first search for a given U_d, the most favorable value of Δ for superconductivity. This is shown in Fig. 19. We see that the susceptibility in the correlated case increases with decreasing Δ faster than the curve for $U_d=0$. The smallest difference is obtained for $\Delta=0$, suggesting that the mixed-valence region is the best candidate for a search of superconductivity.

We show in Fig. 20 results for an extreme mixed-valence case ($U_d=4$, $\Delta=0$). Up to temperatures $T\sim t/4$ we cannot find an enhancement of the pair susceptibility when compared to the uncorrelated case. Simulations at lower temperatures are being carried out presently. To complete our simulation results, we briefly discuss the influence of the two parameters $t_{O\text{-}O}$ and U_p of the model Hamiltonian Eq. (1) not considered yet.

First we show in Fig. 21 results for $t_{O\text{-}O}=0.5$. This value is in agreement with *ab initio* estimates.[40] Since the remaining parameters are the same as for the calculation in Fig. 20, we can directly compare both pictures. The effect of $t_{O\text{-}O}$ is to shift the susceptibility to lower values. The curve for the noninteracting case is also shifted in such a way that no enhancement results. Next we introduce a Hubbard repulsion $U_p=3$ on the oxygen sites (Fig. 22). Compared with Fig. 20 we see, that the correlation curve is shifted to smaller values only very slightly but the difference to the uncorrelated case becomes larger.

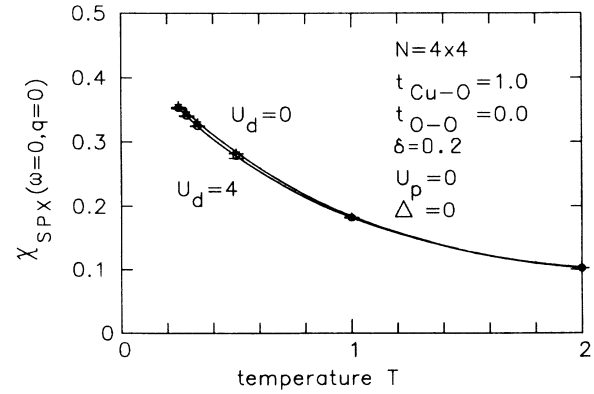

FIG. 20. Pairing susceptibility for a mixed-valence case (extended s wave). We find no enhancement in the considered temperature region.

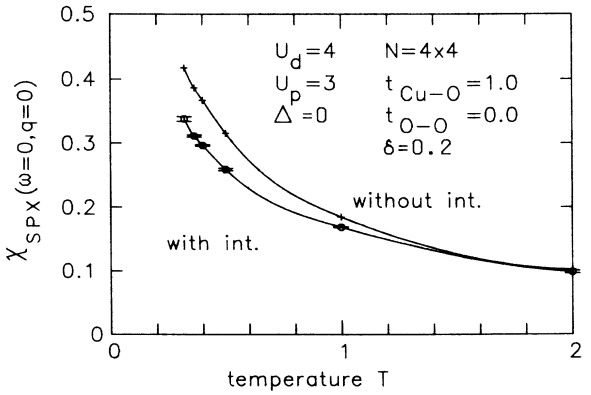

FIG. 22. Pairing susceptibility for the extended s-wave channel. The parameters are the same as in Fig. 20 except that now $U_p=3$.

V. SUMMARY

We presented in this paper a Monte Carlo study of a three-band model that is generally believed to contain the most relevant elements for a description of the CuO_2 layers present in ceramic superconductors.

The simulations were performed using the BSS algorithm complemented with stabilization techniques that at half-filling (one hole per unit cell) allow to reach temperatures as low as $k_B T \sim t/30$ and lower. It is shown by comparison with exact diagonalization results that at such temperatures the ground-state properties of the model are reflected in the simulation. Away from half-filling, massive minus-sign problems are present for $k_B T \lesssim t/10$.

We first discussed several magnetic properties of the model that allowed us to distinguish a charge-transfer region with well-developed magnetic moments on the Cu sites from an itinerant situation where the holes are evenly spread over the unit cell. The local magnetic moments on the Cu sites were shown to be almost independent of doping both in the CT and MV regions. A drastic difference in the structure form factor was found as a function of doping. Whereas a sharp decrease of this quantity is observed in the CT region for doping $\delta \lesssim 0.05$, almost no variation is seen in the MV situation. These results appear natural when studying the electronic compressibility of the system, where a well-developed charge-transfer gap is obtained for $U_d = 6$ and $\Delta = 4$, while no signature of a gap is seen in the MV region ($U_d = 6, \Delta = 1$) up to temperatures as low as $k_B T \sim t/10$. However, the presence of a gap for the MV regime cannot be completely dismissed since a signature for long-range antiferromagnetic order can be observed in the finite-size extrapolation of the structure form factor, where a finite value for the staggered magnetization m_z^2 is obtained in the limit $N \to \infty$ at zero doping. The same extrapolation results in an almost zero value of m_z^2 for a doping of $\delta \approx 0.2$. In the CT region a rather large value of m_z^2 is extrapolated. However, the results of the finite-size studies still have to be confirmed by more extensive calculations since we were able to simulate only moderate lattice sizes (up to 4×4 unit cells). It is interesting to notice that a distinction of a CT regime from a MV regime is already possible for intermediate values of the coupling constants that are in agreement with *ab initio* estimates.

We further studied the formation of a singlet between a hole on a Cu site and a hole on the four nearest-neighbor O sites. We find that the amplitude squared of the singlet per hole on the oxygen sites increases as a function of doping up to $\delta \approx 0.2$, reaching saturation for higher doping.

With respect to superconductivity we find an enhancement of the equal-time correlation function only for the extended s-wave channel for temperatures below $k_B T \sim t/4$ in the MV region. For the CT regime we could not find any enhancement down to temperatures $k_B T \sim t/10$. Unfortunately, minus-sign problems did not allow us to reach lower temperatures with doping. A study of the susceptibilities suggests that the MV region is more favorable for superconductivity but no enhancement was found down to $k_B T \sim t/4$ when compared with the noninteracting (Hartree) ones.

Finally, we briefly showed the effect of the direct O-O hopping $t_{O\text{-}O}$ and a Hubbard coupling U_p on the O sites on the pairing susceptibilities. In both cases a depression occurs and the comparison with the corresponding noninteracting susceptibilities shows no enhancement. Efforts to reach lower temperatures are presently being carried out.

ACKNOWLEDGMENTS

We are grateful to J. Gubernatis, who explained to us the stabilization algorithm, and E. Loh for the exact diagonalization program. We are also grateful to P. Horsch, P. Prelovšek, T. M. Rice, D. J. Scalapino, R. T. Scalettar, H.-B Schüttler, and W. H. Stephan for interesting and clarifying discussions. We kindly acknowledge the Institute for Scientific Interchange (ISI), Torino, Italy, where part of the discussions and calculations took place, for their hospitality and support. Most of the present computations were performed at the HLRZ-Jülich, whose support we kindly acknowledge. Finally we acknowledge support by the BMFT Program No. 13N5501.

*Also at Max-Planck-Institut für Festkörperforschung, D-7000 Stuttgart, Federal Republic of Germany.

[1]G. Bednorz and K. A. Müller, Z. Phys. B **64**, 188 (1986).
[2]D. Vaknin *et al.*, Phys. Rev. Lett. **58**, 2802 (1987); J. M. Tranquada *et al.*, *ibid.* **60**, 156 (1988).
[3]P. W. Anderson, Science **234**, 1196 (1987).
[4]P. W. Anderson, G. Baskaran, Z. Zou, J. Wheatley, T. Hsu, B. S. Shastry, B. Doucot, and S.-D. Liang, Physica C **153-155**, 527 (1988), and references therein.
[5]J. R. Schrieffer, X. G. Wen, and S. C. Zhang, Phys. Rev. Lett. **60**, 944 (1988); Phys. Rev. B **39**, 11 663 (1989).
[6]D. J. Scalapino, E. Loh, and J. E. Hirsch, Phys. Rev. B **34**, 8190 (1986); Phys. Rev. B **35**, 6694 (1987); N. E. Bickers, D. J. Scalapino, and R. T. Scalettar, Int. J. Mod. Phys. B **1**, 687 (1987).
[7]J. Miyake, S. Schmidt-Rink, and C. Varma, Phys. Rev. B **34**, 6554 (1986).
[8]J. C. Fuggle *et al.*, Phys. Rev. B **37**, 123 (1988).
[9]R. L. Kurtz *et al.*, Phys. Rev. B **35**, 8818 (1987).
[10]N. Nücker *et al.*, Phys. Rev. B **37**, 5158 (1988).
[11]V. J. Emery, Phys. Rev. Lett. **58**, 2794 (1987); V. J. Emery and G. Reiter, Phys. Rev. B **38**, 4547 (1988).
[12]J. Zaanen and A. M. Oleś, Phys. Rev. B **37**, 9423 (1988).
[13]A. Muramatsu, R. Zeyher, and D. Schmeltzer, Europhys. Lett. **7**, 473 (1988).
[14]J. E. Hirsch, Phys. Rev. B **31**, 4403 (1985).
[15]S. R. White, R. L. Sugar, and R. T. Scalettar, Phys. Rev. B **38**, 11 665 (1988).

[16]J. E. Hirsch, Phys. Rev. B **38**, 12 023 (1988).
[17]S. R. White, D. J. Scalapino, R. L. Sugar, N. E. Bickers, and R. T. Scalettar, Phys. Rev. B **39**, 839 (1989).
[18]M. Imada, J. Phys. Soc. Jpn. **56**, 3793 (1987); **57**, 42 (1988); **57**, 2689 (1988); **57**, 3128 (1988).
[19]R. T. Scalettar, D. J. Scalapino, R. L. Sugar, and D. Toussaint, Phys. Rev. B **39**, 4711 (1989).
[20]S. Sorella, S. Baroni, R. Car, and M. Parrinello, Europhys. Lett. **8**, 663 (1989).
[21]E. Y. Loh, J. E. Gubernatis, R. T. Scalettar, S. R. White, and R. L. Sugar, in *Workshop on Interacting Electrons in Reduced Dimensions,* edited by D. Baeriswyl and D. K. Campbell (unpublished).
[22]S. R. White, D. J. Scalapino, R. L. Sugar, E. Y. Loh, J. E. Gubernatis, and R. T. Scalettar, Phys. Rev. B **40**, 506 (1989).
[23]R. T. Scalettar, Physica C **162–164**, 313 (1989).
[24]J. E. Hirsch, S. Tang, E. Loh, Jr., and D. J. Scalapino, Phys. Rev. Lett. **60**; J. E. Hirsch, E. Loh, Jr., D. J. Scalapino, and S. Tang, Phys. Rev. B **39**, 243 (1989).
[25]P. Horsch and W. H. Stephan, in *Workshop on Interacting Electrons in Reduced Dimensions,* edited by D. Baeriswyl and D. K. Campbell (unpublished).
[26]J. Bonča, P. Prelovšek, and I. Sega, Phys. Rev. B **39**, 7074 (1989).
[27]J. E. Hirsch and S. Tang, Phys. Rev. Lett. **62**, 591 (1989).
[28]E. Y. Loh and J. E. Gubernatis, in *Electron Phase Transitions,* edited by W. Hanke and Y. V. Kopaev (North-Holland, New York, in press).
[29]E. Y. Loh, J. E. Gubernatis, R. T. Scalettar, S. R. White, D. J. Scalapino, and R. L. Sugar, Phys. Rev. B **41**, 9301 (1990).
[30]R. Blankenbecler, D. J. Scalapino, and R. L. Sugar, Phys. Rev. D **24**, 2278 (1981).
[31]F. C. Zhang and T. M. Rice, Phys. Rev. B **37**, 3795 (1988).
[32]F. C. Zhang, Phys. Rev. B **39**, 7375 (1989).
[33]L. F. Matheiss, Phys. Rev. Lett. **58**, 1028 (1987).
[34]P. B. Littlewood, C. M. Varma, S. Schmidt-Rink, and E. Abrahams, Phys. Rev. B **39**, 12 371 (1989).
[35]R. Putz, B. Ehlers, L. Lilly, A. Muramatsu, and W. Hanke, Phys. Rev. B **41**, 853 (1990).
[36]J. Wagner, A. Muramatsu, and W. Hanke (unpublished).
[37]J. Zaanen, G. A. Sawatzky, and J. W. Allen, Phys. Rev. Lett. **55**, 418 (1985).
[38]W. F. Brinkman and T. M. Rice, Phys. Rev. B **2**, 4302 (1970).
[39]A. M. Oleś and J. Zaanen, Phys. Rev. B **39**, 9175 (1989).
[40]A. K. McMahan, R. M. Martin, and S. Satpathy, Phys. Rev. B **38**, 6650 (1988); M. S. Hybertsen, M. Schluter, and N. E. Christiansen, Phys. Rev. B **39**, 9028 (1989).
[41]P. Prelovšek, Phys. Lett. A **126**, 287 (1988).
[42]N. E. Bickers, D. J. Scalapino, and S. R. White, Phys. Rev. Lett. **62**, 961 (1989).
[43]J.-H. Imer *et al.*, Phys. Rev. Lett. **62**, 336 (1989).
[44]M. Suzuki, Prog. Theor. Phys. **56**, 1454 (1976).
[45]J. E. Hirsch, Phys. Rev. B **28**, 4059 (1983).
[46]J. P. Kogut, Rev. Mod. Phys. **55**, 775 (1983).
[47]R. J. Birgenau *et al.*, Phys. Rev. B **38**, 6614 (1988).
[48]Y. Endoh *et al.*, Phys. Rev. B **37**, 7443 (1988).
[49]J. Oitmaa and D. D. Betts, Can. J. Phys. **56**, 897 (1978).
[50]H. Romberg *et al.*, Z. Phys. B **78**, 367 (1990).